JACS
JOURNAL OF THE AMERICAN CHEMICAL SOCIETY
Article
Cite This: J. Am. Chem. Soc. 2018, 140, 7730−7736
pubs.acs.org/JACS

Highly Emissive Self-Assembled BODIPY-Platinum Supramolecular Triangles

Jiong Zhou,[†,‡] Yuzhen Zhang,[‡] Guocan Yu,[*,†,§] Matthew R. Crawley,[‡] Cressa Ria P. Fulong,[‡] Alan E. Friedman,[∥] Sanghamitra Sengupta,[‡] Jifu Sun,[†] Qing Li,[†] Feihe Huang,[*,†] and Timothy R. Cook[*,‡]

[†]State Key Laboratory of Chemical Engineering, Center for Chemistry of High-Performance and Novel Materials, Department of Chemistry, Zhejiang University, Hangzhou 310027, P. R. China

[‡]Department of Chemistry, University at Buffalo, The State University of New York, Buffalo, New York 14260, United States

[§]Laboratory of Molecular Imaging and Nanomedicine, National Institute of Biomedical Imaging and Bioengineering, National Institutes of Health, Bethesda, Maryland 20892, United States

[∥]Department of Materials Design and Innovation, University at Buffalo, The State University of New York, Buffalo, New York 14260, United States

Supporting Information

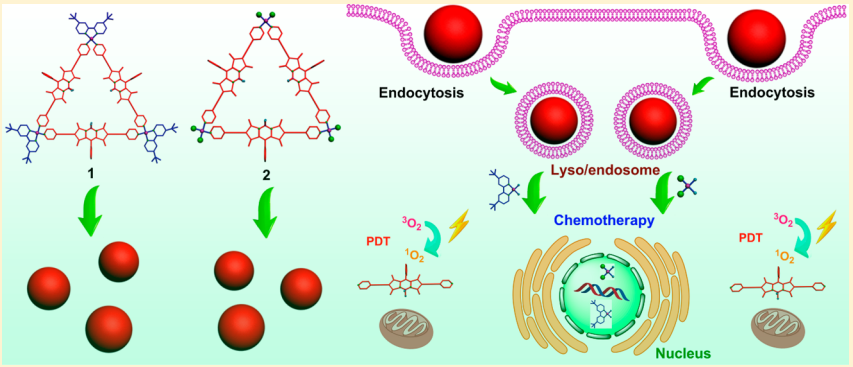

ABSTRACT: Light-emitting supramolecular coordination complexes (SCCs) have been widely studied for applications in the chemical and biological sciences. Herein, we report the coordination-driven self-assembly of two highly emissive platinum(II) supramolecular triangles (**1** and **2**) containing BODIPY-based bridging ligands. The metallacycles exhibit favorable anticancer activities against HeLa cells (IC_{50} of 6.41 and 2.11 μM). The characteristic ∼570 nm fluorescence of the boron dipyrromethene (BODIPY) moieties in the metallacycles permits their intracellular visualization using confocal microscopy. Additionally, the BODIPY fluorophore is an excellent photodynamic agent, making the metallacycles as ideal therapeutics for photodynamic therapy (PDT) and chemotherapy. In vitro studies demonstrate that the combination indexes against HeLa cells are 0.56 and 0.48 for **1** and **2**, respectively, confirming their synergistic anticancer effect. More importantly, these SCCs also exhibit superior anticancer efficacy toward cisplatin-resistant A2780cis cell line by combining PDT and chemotherapy, showing promise in overcoming drug resistance. This study exploits a multicomponent approach to self-assembled metallacages that enables design of effective theranostic agents wherein the platinum acceptors are toxic chemotherapeutics and the BODIPY donors are imaging probes and photosensitizers. Since each piece may be independently tuned, i.e., Pt(II) polypyridyl fragment swapped for Pt(II) phosphine, the activity may be optimized without a total redesign of the system.

INTRODUCTION

Coordination-driven self-assembly is a powerful synthetic methodology providing access to discrete supramolecular coordination complexes (SCCs) with well-defined shapes and sizes by the spontaneous formation of metal−ligand bonds.[1] Owing to the wide range of metals and ligands that are compatible with this strategy, an expansive library of structurally complex two-dimensional (2D) metallacycles and three-dimensional (3D) metallacages has emerged over the past few decades.[2] These metallosupramolecular architectures are of particular interest not only for their aesthetic properties but also because of their extensive applications in catalysis, sensors, supramolecular polymers, amphiphilic self-assembly, host−guest chemistry, and biomedicines.[3] Due to the anticancer activity of organometallic platinum (Pt) complexes and the large number of metallacycles and cages constructed from Pt(II) nodes, biologically active SCCs have emerged in recent

Received: May 13, 2018
Published: May 22, 2018

Downloaded via QUEEN MARY UNIV OF LONDON on March 3, 2022 at 15:44:42 (UTC).
See https://pubs.acs.org/sharingguidelines for options on how to legitimately share published articles.

© 2018 American Chemical Society

DOI: 10.1021/jacs.8b04929
J. Am. Chem. Soc. 2018, 140, 7730−7736

years.[4] Unlike mononuclear clinical drugs, such as cisplatin, imaging capability can also be integrated into these SCC platforms by simply choosing fluorescent ligands as components of the building blocks.[5]

Boron dipyrromethene (BODIPY) dyes have been widely used in photodynamic therapy, bioimaging, chemosensors, and light harvesting.[6] Collectively, BODIPY dyes exhibit numerous favorable properties, including high fluorescence quantum yields, large molar absorption coefficients, easy functionalization, and excellent photostability. Although tetraphenylethene (TPE) and other fluorescent molecules have been used as imaging probes in SCCs,[7] highly emissive SCCs based on BODIPY-containing donors are rare and Pt(II)-BODIPY SCCs have not been explored as theranostic agents.[8] Herein, we report the coordination-driven self-assembly of two novel Pt(II) supramolecular triangles containing a pyridyl-functionalized BODIPY ligand. The presence of Pt(II) ions serving as the metal nodes of triangles provide a mechanism for anticancer activity, resulting in biological activity. The BODIPY cores within triangles enable their transport within cancer cells to be visualized by confocal laser scanning microscopy. Moreover, the BODIPY ligands also form the basis for use as a photosensitizer for photodynamic therapy (PDT). The combination of PDT and chemotherapy greatly enhances anticancer efficacy through a synergistic therapeutic effect. More interestingly, these SCCs exhibited high cytotoxicity against drug resistant cancer cells due to their dual mechanism of action (PDT and chemotherapy), thereby obviating the ubiquitous problem of drug resistance.

RESULTS AND DISCUSSION

Preparation and Characterization of Triangular Metallacycles. The BODIPY ligand **3** was synthesized by a Sonogashira coupling following iodonation of the dye core (Scheme S1). A single crystal of **3** suitable for X-ray diffraction was obtained by slow diffusion of *n*-hexane into the dichloromethane solution at room temperature (Figure 1). In the BODIPY core, the central six-membered ring is almost coplanar with the adjacent five-membered pyrrole rings with the maximum deviations of all non-hydrogen atoms from the mean plane of 0.079 Å, indicating strong π-electron delocalization within the indacene plane.[9] The phenyl ring at the *meso*-position is twisted by 79.61° from the BODIPY plane. The average bond lengths for B−N and B−F and the N−B−N and F−B−F angles are 1.555(2), 1.387(2) Å, 106.8(1), and 109.7(1)°, respectively. The pyridyl rings are also twisted away from the indacene plane. The dihedral angle between the pyridine rings and the indacene plane is 15.66°. See Table S1 for complete crystallographic details. The nearly linear directional nature of **3** makes it an excellent buliding block for SCCs. Treatment of Pt(II) acceptors **4** or **5** with **3** in a 1:1 ratio in CH_2Cl_2/DMA at 60 °C for 24 h led to the formation of self-assembled [3 + 3] triangular metallacycles **1** or **2**, respectively (Scheme 1).

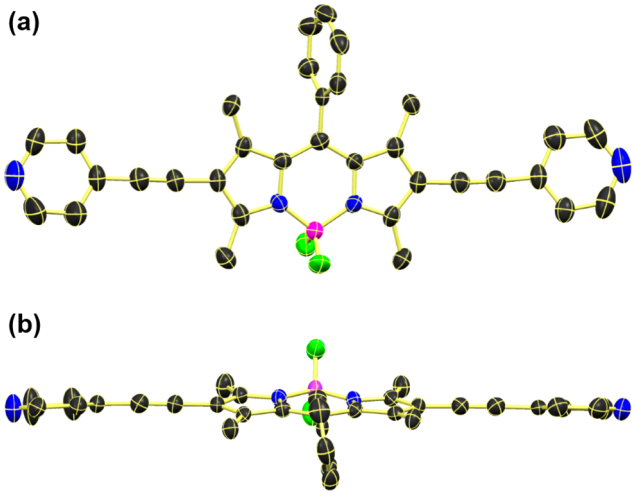

Figure 1. Crystal structure of **3**: (a) side view; (b) top view. Hydrogen atoms are omitted for clarity. Thermal ellipsoid is drawn at 50% probability level. CCDC Number 1569252.

The formation of two triangular metallacycles was supported by multinuclear NMR spectroscopy (^{1}H NMR and ^{31}P{^{1}H} NMR), electrospray ionization mass spectroscopy (ESI-MS), 2D diffusion-ordered spectroscopy (DOSY), UV−vis spectroscopy, and fluorescence spectroscopy. In the ^{1}H NMR spectrum of **1**, the peak corresponding to pyridyl proton H_{3a} (from 8.54 to 8.57 ppm) displayed a downfield shift as compared to that of the free ligand **3**. The peaks for bipyridyl protons H_{4a} (from 8.65 to 8.87 ppm) and H_{4b} (from 8.34 to 8.41 ppm) showed downfield shifts relative to those of Pt(II) acceptor **4** (Figure 2b), consistent with coordination of the N atoms to Pt centers.[8b] Similarly, in the ^{1}H NMR spectrum of **2**, the peak for pyridyl proton H_{3a} (from 8.54 to 8.62 ppm) displayed a downfield shift compared with that of free ligand **3** (Figure 2d). Additionally, the ^{31}P{^{1}H} NMR spectrum of **2** exhibited a lone singlet at −3.04 ppm, consistent with a single phosphorus environment (Figure 2g). This peak was shifted upfield relative to that of Pt(II) acceptor **5** by 7.98 ppm. The well-defined signals in both the ^{1}H NMR and ^{31}P{^{1}H} NMR spectra supported the formation of discrete, highly symmetric species.

Electrospray ionization mass spectrometry (ESI-MS) provided strong evidence for the stoichiometry of formation of triangular metallacycles **1** and **2**. In the mass spectrum of **1**, three peaks were found that were consistent with the assignment of a [3 + 3] assembly (Figures S8 and S9). Among these were a peak at m/z 623.62 corresponding to an intact $[M - 5OTf]^{5+}$ core (Figure 3a). For metallacycle **2**, two such peaks were found (Figures S12 and S13), including a peak at m/z 600.82 corresponding to an intact $[M - 5OTf]^{5+}$ core (Figure 3b). All of these peaks correspond to intact triangular metallacycles that become charged resulting from the loss of triflate counterions. Furthermore, the isotropic distributions were all in good agreement with those predicted from simulation. In a 2D diffusion-ordered spectroscopy (DOSY) experiment, the observation of a single band supports the formation of a single product (Figures S14 and S15). The measured diffusion coefficients of metallacycles **1** and **2** were found to be 4.23×10^{-10} and 4.31×10^{-10} m^2/s, respectively.

Photophysical Studies. The UV−vis absorption spectra of the BODIPY ligand **3** and triangular metallacycles **1** and **2** were recorded in solvents with different polarities (Figures S21a, S22a, and S23a). The spectra showed similar absorption bands at around 556 nm, which was attributed to the $\pi-\pi^*$ transition of the BODIPY moieties.[8c]

The fluorescence properties of the BODIPY ligand **3** and triangular metallacycles **1** and **2** were also studied in a range of solvents (Figures S21b, S22b, and S23b). Metallacycles **1** and **2** were highly fluorescent when excited at 365 nm and showed an emission peak at ∼577 nm, originating from the BODIPY cores (Figure 4). Both triangles showed small shifts in their emission

DOI: 10.1021/jacs.8b04929
J. Am. Chem. Soc. 2018, 140, 7730−7736

Scheme 1[a]

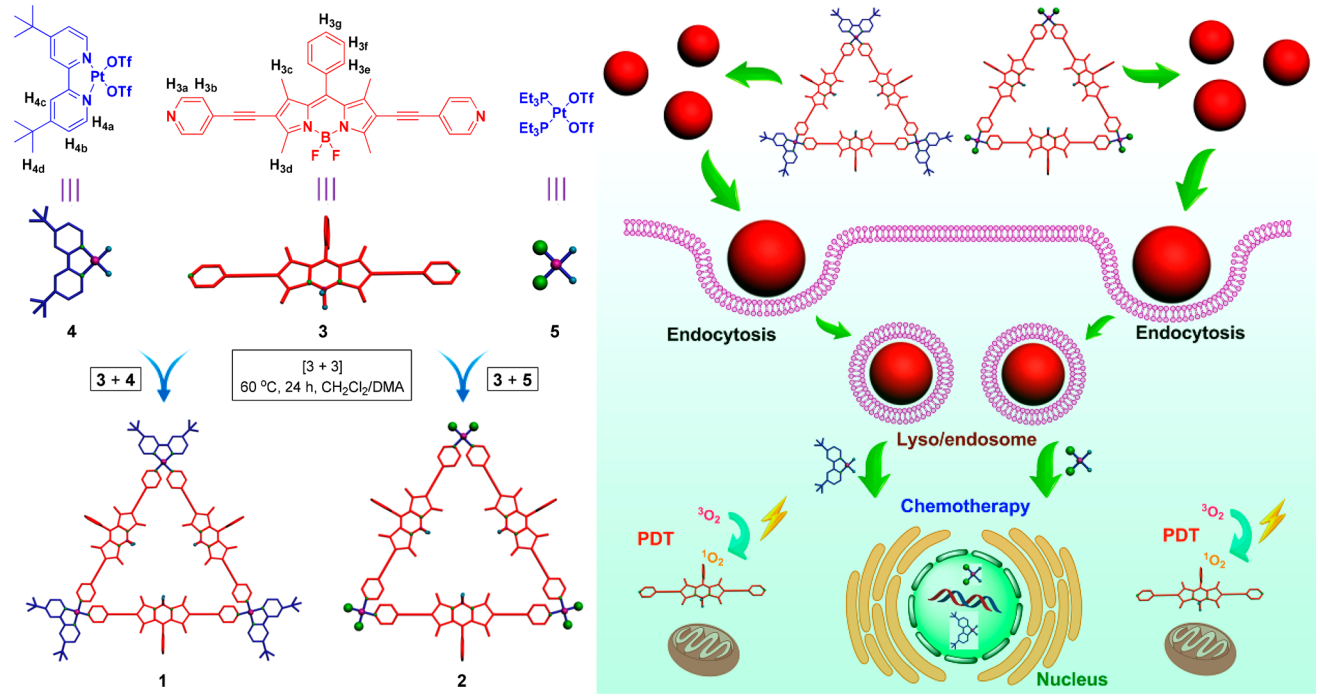

[a](Left) Structures of **3**–**5** and self-assembled triangular metallacycles **1** and **2**. (Right) Cartoon illustration of the cellular uptake of nanoparticles prepared from **1** and **2**.

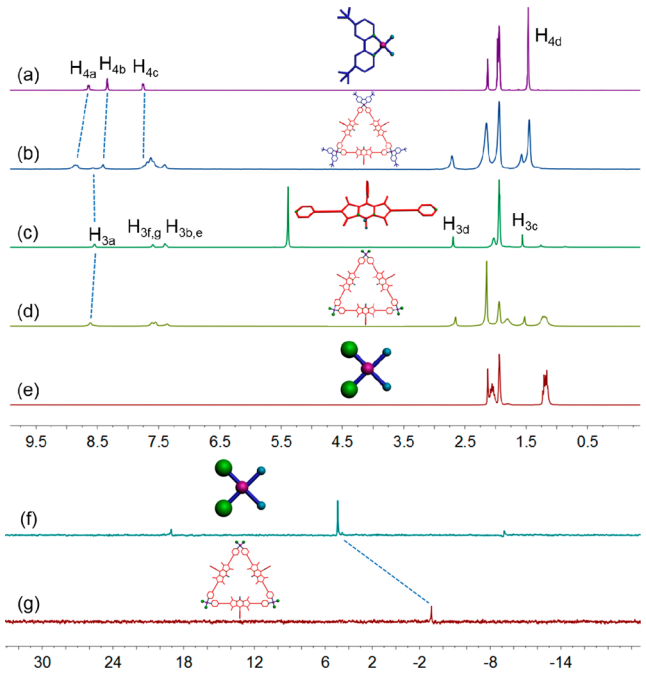

Figure 2. (a–e) ^{1}H NMR and (f,g) ^{31}P{^{1}H} NMR spectra (acetonitrile-d_3, 293 K) of free building blocks **4** (a), **3** (c), and **5** (e,f) and triangular metallacycles **1** (b) and **2** (d,g).

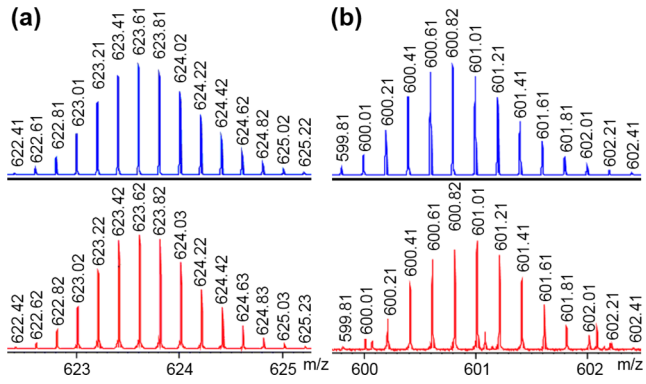

Figure 3. Experimental (red) and calculated (blue) ESI-MS spectra of (a) **1** $[M - 5OTf]^{5+}$ and (b) **2** $[M - 5OTf]^{5+}$.

maxima depending on the solvent used (Figure S24). Using Rhodamine B (Φ_F = 31% in water) as a standard,[10] the quantum yields (Φ_F) of ligand **3** and triangular metallacycles **1** and **2** were determined in different solvents (Table S2). Although some variation was observed, we note that in all cases the emission quantum yields remained high. It has been observed that if the Pt(II) nodes are too close to the BODIPY cores, emission may be quenched, presumably due to the heavy-metal effect that populates dark triplet states. Introducing ethynyl spacers to move the Pt(II) centers further away has been observed to limit the attenuation of quantum yield.[8a]

Cell Imaging and in Vitro Anticancer Treatment. Nanoparticles (NPs) containing metallacycle **1** or **2** were prepared through nanoprecipitation.[5a] Solution of these NPs of **1** or **2** exhibited a clear Tyndall effect (Figure S27 insets), supporting the existence of nanoaggregates. Transmission electron microscopy (TEM) and dynamic light scattering (DLS) techniques were used to reveal the morphology and size of these nanostructures. Solid spherical structures with an average diameter of ~40 nm formed from **1** were observed in the TEM image (Figure S26a). In DLS experiment, a unimodal peak distribution with an effective average hydrodynamic diameter of 42 nm was observed (Figure S27a), in good agreement with the result obtained from TEM experiments. Metallacycle **2** also formed spherical aggregates with diameters

DOI: 10.1021/jacs.8b04929
J. Am. Chem. Soc. 2018, 140, 7730–7736

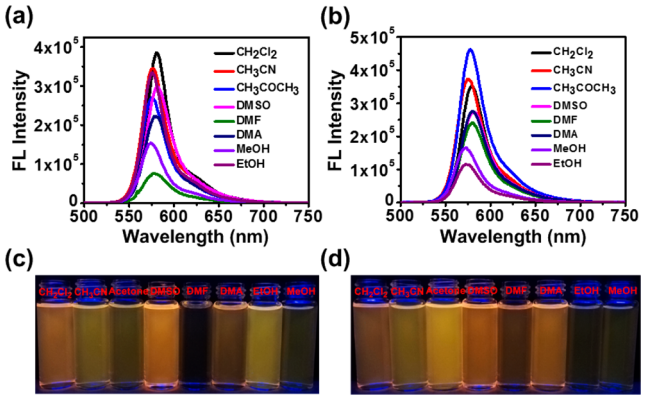

Figure 4. Fluorescence emission spectra of metallacycles **1** (a) and **2** (b) in different solvents (λ_{ex} = 556 nm, c = 1.00 μM). Photographs of **1** (c) and **2** (d) under UV lamp at 365 nm in different solvents (c = 1.00 μM). DMSO, dimethylsulfoxide; DMF, dimethylformamide; DMA, dimethylacetamide.

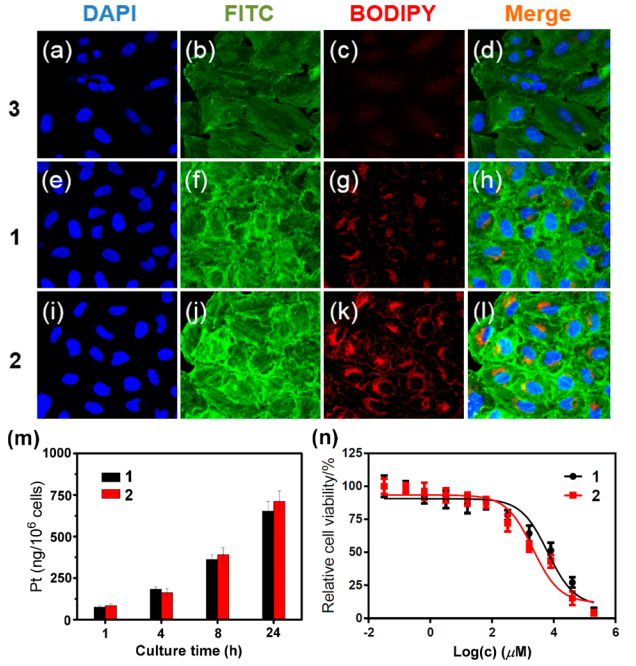

Figure 5. CLSM images of HeLa cells after incubation with the ligand **3** and metallacycles **1** and **2** for 8 h: (a,e,i) stained with DAPI (nucleus); (b,f,j) stained with FITC (β-actin); (c,g,k) fluorescent image; (d) merged image from (a), (b), and (c); (h) merged image from (e), (f), and (g); (l) merged image from (i), (j), and (k). (m) Quantitative analysis of the Pt amounts in HeLa cells after incubation with metallacycles **1** and **2** for 1, 4, 8, and 24 h, respectively. (n) Cytotoxicity of metallacycles **1** and **2** toward HeLa cells after 24 h incubation.

of ~45 nm (Figure S26b). Similar DLS experiment showed an average diameter of ~48 nm (Figure S27b), consistent with the TEM measurements. Furthermore, the in vitro stability of the nanoparticles was evaluated in phosphate-buffered saline (PBS) containing 10% fetal bovine serum (FBS) at 37 °C. No obvious size variations were observed over 20 h, confirming the excellent stability of these NPs under physiological conditions (Figure S28).

Confocal laser scanning microscopic (CLSM) and flow cytometry (FCM) investigations were carried out to confirm that the NPs containing the metallacycles **1** or **2** were internalized by human cervical cancer cells (HeLa).[5a] Cells were counterstained with 4′,6-diamidino-2-phenylindole (DAPI) or fluorescein isothiocyanate (FITC)-labeled phalloidin to differentiate the nuclear or cytoplasmic region. As shown in Figure 5, the HeLa cells exhibited strong intracellular fluorescence after incubation with the NPs containing the metallacycles **1** or **2** for 8 h. The amount of the NPs containing the metallacycles **1** or **2** internalized by HeLa cells was quantified by FCM (Figure S31). The mean fluorescence intensity arising from **1** or **2** was much higher than that of the BODIPY ligand **3** under the same conditions, indicating that HeLa cells had a faster uptake rate and higher intracellular accumulation after incubation with the NPs containing metallacycle **1** or **2**. For example, HeLa cells ingested about four times the amount of the NPs containing metallacycle **1** or **2** than the BODIPY ligand **3** after incubation for 4 h. The reason was that the cationic nature of the NPs was favorable for the cellular internalization because the potential of cell membrane is negative (Figures S29 and S30).[11]

Inductively coupled plasma optical emission spectrometry (ICP-OES) was performed to determine the amounts of Pt internalized by HeLa cells after incubation with metallacycles **1** and **2**.[12] The amounts of Pt in cells treated with both SCCs continued to increase over 24 h (Figures 5m and S33). For **1**, the accumulation of Pt in HeLa cells was determined to be 653 ng/10^6 cells after 24 h incubation. For **2**, the accumulation of Pt in HeLa cells was determined to be 713 ng/10^6 cells after 24 h incubation, which was much higher than that of free Pt(II) acceptor **5** (274 ng/10^6 cells). These observations indicated that the cellular uptakes of Pt complexes were improved by formation of metallacycles.

The cytotoxicities of Pt(II) acceptors **4** and **5** and metallacycles **1** and **2** against HeLa cells were evaluated by a 3-(4′,5′-dimethylthiazol-2′-yl)-2,5-diphenyltetrazolium bromide (MTT) assay with different concentrations (Figure 5n and Table S3). Cisplatin was used as a standard drug in killing HeLa cancer cells with the 50% growth inhibitory concentration (IC_{50}) value (0.81 μM). Metallacycle **1** displayed potent cytotoxicity, with the IC_{50} value (6.41 μM) comparable to that of free Pt(II) acceptor **4** (3.60 μM). For metallacycle **2**, the IC_{50} value was 2.11 μM, which was also comparable to that of free Pt(II) acceptor **5** (1.76 μM). For United States Food and Drug Administration (FDA)-approved platinum-based anticancer drugs, such as cisplatin, carboplatin, and oxaliplatin, their nonfluorescent nature becomes an obstacle for tracking the processes of translocation, drug release, and excretion of anticancer agents. The introduction of BODIPY into the SCCs introduces a fluorophore which is absent from traditional Pt-based drugs, thereby enabling fluorescence imaging-guided cancer therapy.

In Vitro Photodynamic Therapy. Benefiting from their easy modifications, low dark toxicities, high photostability, sharp fluorescence emissions with high fluorescence quantum yields, and high extinction coefficients, BODIPY derivatives are ideal photodynamic agents for cancer PDT.[13] The generation of singlet oxygen ($^1O_2$) by the metallacycles was monitored by using singlet oxygen sensor green (SOSG) as a probe with highly selectivity for $^1O_2$. The fluorescence of SOSG is silent in its intact form while becomes much brighter after reaction with $^1O_2$. As shown in Figures 6c and S34, the fluorescence emission at 532 nm increased rapidly upon light irradiation, confirming

DOI: 10.1021/jacs.8b04929
J. Am. Chem. Soc. 2018, 140, 7730−7736

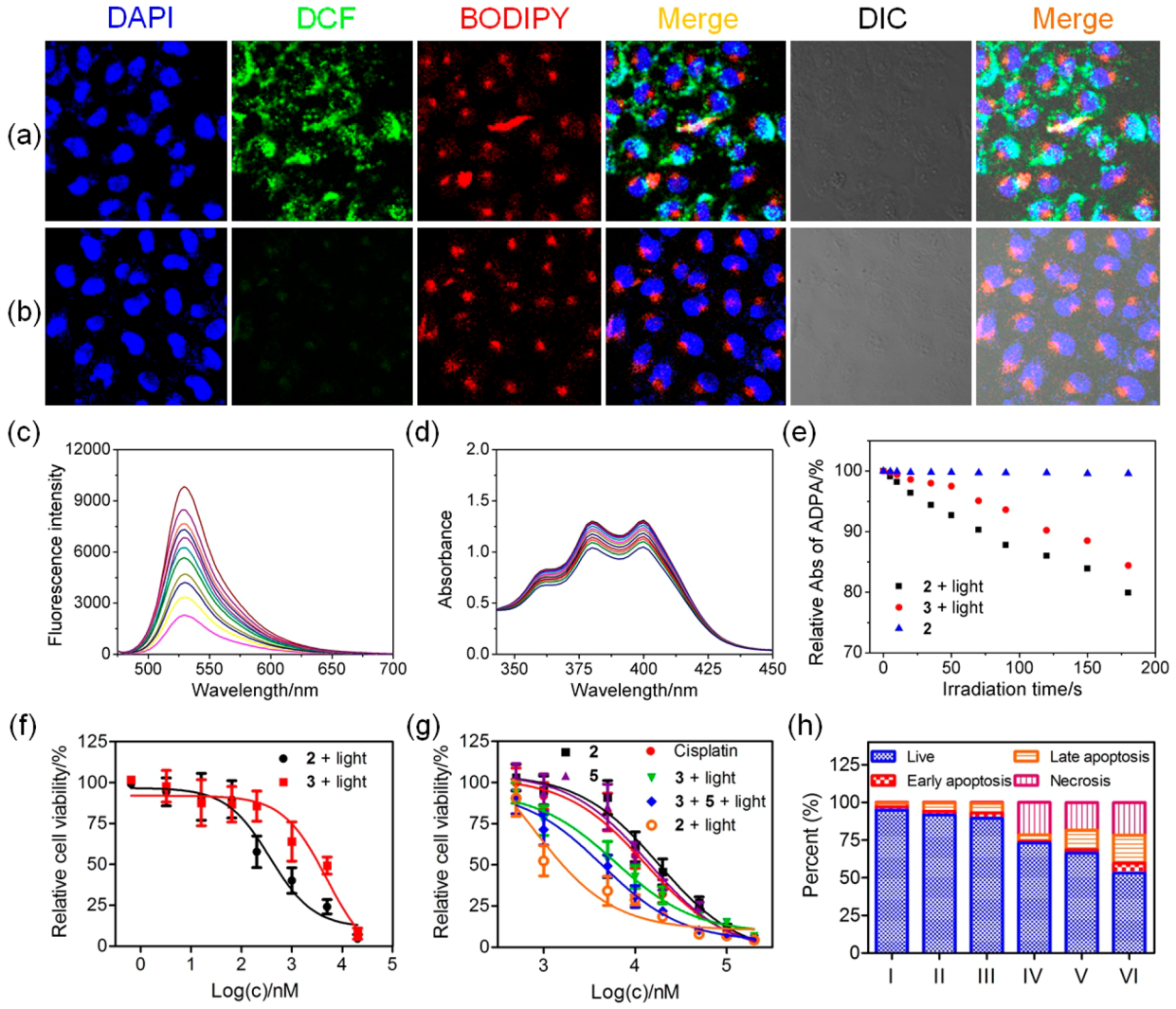

Figure 6. CLSM images of HeLa cells after incubation with **2** and DCF-DA in the (a) absence and (b) presence of vitamin C. (c) Fluorescence enhancement of a SOSG solution by $^1O_2$ generated by **2**. (d) UV−vis spectra of APDA in the presence of **2** upon light irradiation (400−700 nm, 50 mW/cm^2) for different times. (e) Relative absorbance changes of APDA at 378 nm with 500 nM **2** or **3** in the light and dark. (f) Cytotoxicity of **2** and **3** against HeLa cells with light irradiation. (g) Cytotoxicity of different formulations against drug resistant A2780cis cells. (h) Flow cytometric analysis of Annexin-V/PI dual-staining of HeLa cells after different treatments (I, **2**; II, **5**; III, cisplatin; IV, **3** + light; V, **3** + **5** + light; VI, **2** + light). The concentration of the formulations was 1.00 μM.

the successful generation of $^1O_2$. Anthracene-9,10-dipropionic acid disodium (ADPA) was employed as an indicator to further demonstrate the singlet oxygen generation. Negligible changes in ADPA absorption was observed for the metallacycles without light irradiation, while a gradual decrease in ADPA absorption occurred upon irradiation of the aqueous solution containing the photosensitizers (Figures 6d and S35), an indication of singlet oxygen generation. In comparison, the relative changes in ADPA absorbance of BODIPY ligand **3** was slower than those of the metallacycles (Figures 6e and S36), suggesting better $^1O_2$ generation ability by the formation of metallacycles.

To assess the intracellular $^1O_2$ generation by these SCCs after internalization, dichlorofluorescein diacetate (DCF-DA) was chosen as an oxidant-sensitive fluorescent dye to detect the formed reactive oxygen species, which rapidly oxidized DCF-DA into highly fluorescent dichlorofluorescein (DCF). For the cells cultured with the SCCs, strong green fluorescence signal from DCF was monitored inside the cells upon light irradiation (Figures 6a and S37a), which was indicative of efficient $^1O_2$ generation. In contrast, the fluorescence signal related to DCF significantly decreased by pretreating the cells with reactive oxygen species scavenger vitamin C (50 μM) (Figures 6b and S37b), further verifying the intracellular $^1O_2$ production in the presence of light irradiation.

Encouraged by these observations, we evaluated the synergistic anticancer effect of these SCCs against HeLa cells. The IC_{50} value of **3** was determined to be 4.88 μM upon light irradiation (Figure 6f). Excitingly, the IC_{50} values of **1** and **2** were decreased to 0.95 and 0.37 μM, respectively. Compared with these data, we knew that **2** exhibited better anticancer efficacy, possibly arising from its higher cytotoxicity and more internalization efficiency. The combination indexes (CI) were calculated to be 0.56 and 0.48, respectively. The CI values are much lower than 1, suggesting excellent synergistic effect is achieved for the SCCs integrating PDT and chemotherapy.

Drug resistance, both inherent and acquired, is the main reason for the failure of platium-based anticancer drugs, greatly limiting their utility in cancer treatments. In order to enhance

DOI: 10.1021/jacs.8b04929
J. Am. Chem. Soc. 2018, 140, 7730−7736

the anticancer efficacy, combination therapy is widely employed to combat drug resistance by "collecting" the merits of different therapeutic modalities. PDT using the generated $^1O_2$ to incude cell apoptosis/necosis by oxidating DNA/proteins inside cells, is an ideal complementary treatment to chemotherapy, thus realizing synergetic anticancer efficacy to overcome drug resistance through a multipronged assault. From MTT assay shown in Figure 6g, the IC_{50} values against drug resistant A2780cis cells were measured to be 12.9, 14.2, 18.1, 6.09, 4.43, and 0.76 μM for cisplatin, **5**, **2**, **3** + light, **3** + **5** + light, and **2** + light, respectively. In vitro toxicity studies demonstrated that the combination of PDT and chemotherapy (**2** + light) was up to 1 order of magnitude more potent than the chemotherapy alone (**2**), and its cytotoxicity was around 9-fold higher than that of the FDA-approved cisplatin, confirming the outstanding anticancer efficacy against drug-resistant cancer cell. Compared with the metallacycle, the anticancer efficacy decreased effectively by simply mixing the chemotherapeutic and photosensitizer upon light irradiation (**3** + **5** + light) because of its relatively low internalization and photodynamic effect, which emphasized that the formation of metallacycle played a vital role in enhancing its anticancer performance. Moreover, the CI value of **2** + light was calculated to be 0.84, which verified its remarkable synergistic effect.

In order to provide more information of the synergetic efficacy of PDT and chemotherapy, Annexin-V FITC and propidium iodide (PI) dual-staining assay was conducted to quantitatively distinguish viable cells from dead cells by flow cytometry. Due to their low anticancer efficacy against A2780cis cells, chemotherapy alone (cisplatin, **5**, or **2**) rarely induced cell apoptosis (Figure 6h). For PDT alone, a total of 26.7% A2780cis cells showed apoptosis/necrosis after irradiation for 5 min with the power of 50 mW/cm^2. Additionally, the apoptotic/necrotic percentage increased to 33.6% for the cells treated with the mixture of **3** and **5** followed by irradiation. Notably, the population of apoptotic and necrotic cells treated with **2** + light was 46.9%, much higher than the other formulations, in good agreement with the results obtained from MTT assay. Similarly, metallacycle **1** also exhibited superior anticancer efficacy and synergistic effect against A2780cis cells (Figures S38 and S39). Together, these studies demonstrated that these metallacycles **1** and **2** exhibited potential applications in imaging-guided cancer therapy, endowing the platinum-based chemotherapeutic agents with diagnostic/imaging capability, which could be used to trace their delivery, release, and efficacy.

CONCLUSIONS

In summary, we report here the first examples of highly emissive Pt(II) supramolecular triangles bearing a pyridine-functionalized BODIPY ligand via coordination-driven self-assembly for theranostic studies. The formation of two triangular metallacycles was fully characterized by multinuclear NMR (^{1}H and ^{31}P), ESI-MS, 2D DOSY, UV−vis spectroscopy, and fluorescence spectroscopy. These triangles possessed promising potential applications in cancer theranostics, in which the platinum acceptors were toxic chemotherapeutics and the BODIPY donor was imaging probe and photosensitizer. In vitro studies demonstrated that the formation of metallacycles improved their anticancer efficacy, and the combination of PDT and chemotherapy showed excellent synergistic effect. More importantly, these SCCs exhibited superior anticancer outcomes against drug resistant A2780cis cells integrating two different therapeutic modalities into the supramolecular platforms. The self-assembled BODIPY-platinum supramolecular triangles provides a promising platform for fluorescence imaging-guided cancer therapy.

ASSOCIATED CONTENT

Supporting Information

The Supporting Information is available free of charge on the ACS Publications website at DOI: 10.1021/jacs.8b04929.

Experimental details, NMR spectra, and other materials (PDF)
Crystal data for **3** (CIF)
Crystal data for **7** (CIF)

AUTHOR INFORMATION

Corresponding Authors

*guocanyu@zju.edu.cn
*fhuang@zju.edu.cn
*trcook@buffalo.edu

ORCID

Yuzhen Zhang: 0000-0003-2763-9798
Matthew R. Crawley: 0000-0002-2555-9543
Cressa Ria P. Fulong: 0000-0002-5574-7609
Alan E. Friedman: 0000-0002-4764-8168
Jifu Sun: 0000-0001-7536-9759
Feihe Huang: 0000-0003-3177-6744
Timothy R. Cook: 0000-0002-7668-8089

Notes

The authors declare no competing financial interest.

ACKNOWLEDGMENTS

F.H. thanks the National Natural Science Foundation of China (21434005) and the Fundamental Research Funds for the Central Universities for financial support. T.R.C. thanks the University at Buffalo and the State University of New York (SUNY) Research Foundation, SUNY Fredonia for the use of their X-ray diffractometer, and the National Center for Research Resources (S10RR029517) for financial support.

REFERENCES

(1) (a) Fujita, M.; Tominaga, M.; Hori, A.; Therrien, B. *Acc. Chem. Res.* **2005**, *38*, 369−378. (b) Oliveri, C. G.; Ulmann, P. A.; Wiester, M. J.; Mirkin, C. A. *Acc. Chem. Res.* **2008**, *41*, 1618−1629. (c) Chakrabarty, R.; Mukherjee, P. S.; Stang, P. J. *Chem. Rev.* **2011**, *111*, 6810−6918. (d) Cook, T. R.; Zheng, Y.-R.; Stang, P. J. *Chem. Rev.* **2013**, *113*, 734−777. (e) Cook, T. R.; Stang, P. J. *Chem. Rev.* **2015**, *115*, 7001−7045. (f) McConnell, A. J.; Wood, C. S.; Neelakandan, P. P.; Nitschke, J. R. *Chem. Rev.* **2015**, *115*, 7729−7793. (g) Yamashina, M.; Sartin, M. M.; Sei, Y.; Akita, M.; Takeuchi, S.; Tahara, T.; Yoshizawa, M. *J. Am. Chem. Soc.* **2015**, *137*, 9266−9269. (h) Yan, X.; Cook, T. R.; Wang, P.; Huang, F.; Stang, P. J. *Nat. Chem.* **2015**, *7*, 342−348. (i) Oldacre, A. N.; Friedman, A. E.; Cook, T. R. *J. Am. Chem. Soc.* **2017**, *139*, 1424−1427. (j) Gupta, G.; Das, A.; Panja, S.; Ryu, J. Y.; Lee, J.; Mandal, N.; Lee, C. Y. *Chem. - Eur. J.* **2017**, *23*, 17199−17203.

(2) (a) Therrien, B.; Süss-Fink, G.; Govindaswamy, P.; Renfrew, A. K.; Dyson, P. J. *Angew. Chem., Int. Ed.* **2008**, *47*, 3773−3776. (b) Chen, L.-J.; Ren, Y.-Y.; Wu, N.-W.; Sun, B.; Ma, J.-Q.; Zhang, L.; Tan, H.; Liu, M.; Li, X.; Yang, H.-B. *J. Am. Chem. Soc.* **2015**, *137*, 11725−11735. (c) Frischmann, P. D.; Kunz, V.; Würthner, F. *Angew. Chem., Int. Ed.* **2015**, *54*, 7285−7289. (d) Gupta, G.; Das, A.; Ghate, N. B.; Kim, T.; Ryu, J. Y.; Lee, J.; Mandal, N.; Lee, C. Y. *Chem. Commun.* **2016**, *52*, 4274−4277. (e) Zhou, Z.; Yan, X.; Saha, M. L.; Zhang, M.; Wang, M.; Li, X.; Stang, P. J. *J. Am. Chem. Soc.* **2016**, *138*,

DOI: 10.1021/jacs.8b04929
J. Am. Chem. Soc. 2018, 140, 7730−7736

13131−13134. (f) Samanta, S. K.; Moncelet, D.; Briken, V.; Isaacs, L. *J. Am. Chem. Soc.* **2016**, *138*, 14488−14496. (g) Zhang, Y.; Crawley, M. R.; Hauke, C. E.; Friedman, A. E.; Cook, T. R. *Inorg. Chem.* **2017**, *56*, 4258−4262. (h) Zheng, W.; Yang, G.; Shao, N.; Chen, L.-J.; Ou, B.; Jiang, S.-T.; Chen, G.; Yang, H.-B. *J. Am. Chem. Soc.* **2017**, *139*, 13811−13820.

(3) (a) Li, S.; Huang, J.; Cook, T. R.; Pollock, J. B.; Kim, H.; Chi, K.-W.; Stang, P. J. *J. Am. Chem. Soc.* **2013**, *135*, 2084−2087. (b) Yan, X.; Li, S.; Cook, T. R.; Ji, X.; Yao, Y.; Pollock, J. B.; Shi, Y.; Yu, G.; Li, J.; Huang, F.; Stang, P. J. *J. Am. Chem. Soc.* **2013**, *135*, 14036−14039. (c) Yan, X.; Cook, T. R.; Pollock, J. B.; Wei, P.; Zhang, Y.; Yu, Y.; Huang, F.; Stang, P. J. *J. Am. Chem. Soc.* **2014**, *136*, 4460−4463. (d) Li, S.; Huang, J.; Zhou, F.; Cook, T. R.; Yan, X.; Ye, Y.; Zhu, B.; Zheng, B.; Stang, P. J. *J. Am. Chem. Soc.* **2014**, *136*, 5908−5911. (e) Ye, Y.; Cook, T. R.; Wang, S.-P.; Wu, J.; Li, S.; Stang, P. J. *J. Am. Chem. Soc.* **2015**, *137*, 11896−11899. (f) Zhou, J.; Yu, G.; Huang, F. *Chem. Soc. Rev.* **2017**, *46*, 7021−7053.

(4) (a) Cook, T. R.; Vajpayee, V.; Lee, M. H.; Stang, P. J.; Chi, K.-W. *Acc. Chem. Res.* **2013**, *46*, 2464−2474. (b) Grishagin, I. V.; Pollock, J. B.; Kushal, S.; Cook, T. R.; Stang, P. J.; Olenyuk, B. Z. *Proc. Natl. Acad. Sci. U. S. A.* **2014**, *111*, 18448−18453. (c) Chan, A. K.-W.; Lam, W. H.; Tanaka, Y.; Wong, K. M.-C.; Yam, V. W.-W. *Proc. Natl. Acad. Sci. U. S. A.* **2015**, *112*, 690−695. (d) Zheng, Y.-R.; Suntharalingam, K.; Johnstone, T. C.; Lippard, S. J. *Chem. Sci.* **2015**, *6*, 1189−1193.

(5) (a) Yu, G.; Cook, T. R.; Li, Y.; Yan, X.; Wu, D.; Shao, L.; Shen, J.; Tang, G.; Huang, F.; Chen, X.; Stang, P. J. *Proc. Natl. Acad. Sci. U. S. A.* **2016**, *113*, 13720−13725. (b) Yu, G.; Zhang, M.; Saha, M. L.; Mao, Z.; Chen, J.; Yao, Y.; Zhou, Z.; Liu, Y.; Gao, C.; Huang, F.; Chen, X.; Stang, P. J. *J. Am. Chem. Soc.* **2017**, *139*, 15940−15949.

(6) (a) Lee, C. Y.; Farha, O. K.; Hong, B. J.; Sarjeant, A. A.; Nguyen, S. T.; Hupp, J. T. *J. Am. Chem. Soc.* **2011**, *133*, 15858−15861. (b) Musser, A. J.; Neelakandan, P. P.; Richter, J. M.; Mori, H.; Friend, R. H.; Nitschke, J. R. *J. Am. Chem. Soc.* **2017**, *139*, 12050−12059.

(7) (a) Zhang, M.; Li, S.; Yan, X.; Zhou, Z.; Saha, M. L.; Wang, Y.-C.; Stang, P. J. *Proc. Natl. Acad. Sci. U. S. A.* **2016**, *113*, 11100−11105. (b) Saha, M. L.; Yan, X.; Stang, P. J. *Acc. Chem. Res.* **2016**, *49*, 2527−2539.

(8) (a) Kaloudi-Chantzea, A.; Karakostas, N.; Raptopoulou, C. P.; Psycharis, V.; Saridakis, E.; Griebel, J.; Hermann, R.; Pistolis, G. *J. Am. Chem. Soc.* **2010**, *132*, 16327−16329. (b) Zhang, M.; Saha, M. L.; Wang, M.; Zhou, Z.; Song, B.; Lu, C.; Yan, X.; Li, X.; Huang, F.; Yin, S.; Stang, P. J. *J. Am. Chem. Soc.* **2017**, *139*, 5067−5074. (c) Gupta, G.; Das, A.; Park, K. C.; Tron, A.; Kim, H.; Mun, J.; Mandal, N.; Chi, K.-W.; Lee, C. Y. *Inorg. Chem.* **2017**, *56*, 4615−4621.

(9) (a) Ulrich, G.; Ziessel, R.; Harriman, A. *Angew. Chem., Int. Ed.* **2008**, *47*, 1184−1201. (b) Yin, X.; Li, Y.; Zhu, Y.; Jing, X.; Li, Y.; Zhu, D. *Dalton Trans.* **2010**, *39*, 9929−9935.

(10) Williams, A. T. R.; Winfield, S. A.; Miller, J. N. *Analyst* **1983**, *108*, 1067−1071.

(11) (a) Sun, C.-Y.; Shen, S.; Xu, C.-F.; Li, H.-J.; Liu, Y.; Cao, Z.-T.; Yang, X.-Z.; Xia, J.-X.; Wang, J. *J. Am. Chem. Soc.* **2015**, *137*, 15217−15224. (b) Li, H.-J.; Du, J.-Z.; Du, X.-J.; Xu, C.-F.; Sun, C.-Y.; Wang, H.-X.; Cao, Z.-T.; Yang, X.-Z.; Zhu, Y.-H.; Nie, S.; Wang, J. *Proc. Natl. Acad. Sci. U. S. A.* **2016**, *113*, 4164−4169.

(12) Xiao, H.; Qi, R.; Liu, S.; Hu, X.; Duan, T.; Zheng, Y.; Huang, Y.; Jing, X. *Biomaterials* **2011**, *32*, 7732−7739.

(13) Kamkaew, A.; Lim, S. H.; Lee, H. B.; Kiew, L. V.; Chung, L. Y.; Burgess, K. *Chem. Soc. Rev.* **2013**, *42*, 77−88.

DOI: 10.1021/jacs.8b04929
J. Am. Chem. Soc. 2018, 140, 7730−7736